Published in final edited form as:
Blood. 2012 June 14; 119(24): 5931–5942. doi:10.1182/blood-2011-12-396895.

Aberrant mural cell recruitment to lymphatic vessels and impaired lymphatic drainage in a murine model of pulmonary fibrosis

Anna-Katharina Meinecke[1], **Nadine Nagy**[2], **Gabriela D'Amico Lago**[3], **Santina Kirmse**[1], **Ralph Klose**[1], **Katrin Schrödter**[1], **Annika Zimmermann**[2], **Iris Helfrich**[4], **Helene Rundqvist**[5], **Dirk Theegarten**[6], **Olaf Anhenn**[7], **Véronique Orian-Rousseau**[8], **Randall S. Johnson**[9], **Kari Alitalo**[3], **Jens W. Fischer**[2], **Joachim Fandrey**[1], and **Christian Stockmann**[1]

[1]Institut für Physiologie, University Hospital Essen, University Duisburg-Essen, Essen, Germany [2]Institut für Pharmakologie und Klinische Pharmakologie, University Hospital Düsseldorf, Heinrich-Heine-University Düsseldorf, Düsseldorf, Germany [3]Molecular Cancer Biology Program, Biomedicum Helsinki, Haartman Institute, University of Helsinki, Helsinki, Finland [4]Department of Dermatology, University Hospital Essen, Essen, Germany [5]Department of Oncology & Pathology, Karolinska Institutet, Stockholm, Sweden [6]Departments of Pathology and Neuropathology, University Hospital Essen, University Duisburg-Essen, Essen, Germany [7]Departments of Pneumology, West German Lung Centre, University Hospital Essen, University Duisburg-Essen, Essen, Germany [8]Karlsruhe Institute of Technology, Institute for Toxocology and Genetics, Karlsruhe, Germany [9]Molecular Biology Section, Division of Biology, University of California, San Diego, San Diego, CA

Abstract

Pulmonary fibrosis is a progressive disease with unknown etiology that is characterized by extensive remodeling of the lung parenchyma, ultimately resulting in respiratory failure. Lymphatic vessels have been implicated with the development of pulmonary fibrosis, but the role of the lymphatic vasculature in the pathogenesis of pulmonary fibrosis remains enigmatic. Here we show in a murine model of pulmonary fibrosis that lymphatic vessels exhibit ectopic mural coverage and that this occurs early during the disease. The abnormal lymphatic vascular patterning in fibrotic lungs was driven by expression of platelet-derived growth factor B (PDGF-B) in lymphatic endothelial cells and signaling through platelet-derived growth factor receptor (PDGFR)–β in associated mural cells. Because of impaired lymphatic drainage, aberrant mural

Correspondence: Christian Stockmann, Institut für Physiologie, University Hospital Essen, University of Duisburg-Essen, Hufelandstrasse 55, 45122 Essen, Germany; christian.stockmann@uni-due.de.

Authorship

Contribution: A.-K.M. performed research, collected, analyzed and interpreted data and wrote the paper; N.N. performed research and analyzed data; G.D.L. performed research and contributed vital new reagents; S.K., R.K., and K.S. performed research; A.Z. contributed analytical tools; I.H. contributed vital new reagents; H.R. contributed analytical tools; D.T., O.A., and V.O.-R. contributed vital new reagents; R.S.J., K.A., J.W.F., and J.F. analyzed and interpreted data and designed research; C.S. performed research, collected, analyzed and interpreted data, designed research, and wrote the paper.

Conflict-of-interest disclosure: The authors declare no competing financial interests.

The publication costs of this article were defrayed in part by page charge payment. Therefore, and solely to indicate this fact, this article is hereby marked "advertisement" in accordance with 18 USC section 1734.

Europe PMC Funders Author Manuscripts

cell coverage fostered the accumulation of fibrogenic molecules and the attraction of fibroblasts to the perilymphatic space. Pharmacologic inhibition of the PDGF-B/PDGFR-β signaling axis disrupted the association of mural cells and lymphatic vessels, improved lymphatic drainage of the lung, and prevented the attraction of fibroblasts to the perilymphatic space. Our results implicate aberrant mural cell recruitment to lymphatic vessels in the pathogenesis of pulmonary fibrosis and that the drainage capacity of pulmonary lymphatics is a critical mediator of fibroproliferative changes.

Introduction

Idiopathic pulmonary fibrosis (IPF) is a chronic and progressive lung disease with increasing mortality that ultimately leads to ventilatory restriction and respiratory failure within 3 to 5 years from the time of diagnosis.[1] Pulmonary fibrosis is characterized by extensive remodeling of the lung parenchyma, including accumulation of fibroblasts and connective tissue overgrowth.[2] However, the pathogenetic events that trigger this process remain enigmatic and there has been little progress in the development of therapeutic strategies for this disease.

Vascular remodeling is a hallmark observation during pulmonary fibrosis and recent studies indicate that pulmonary lymphatics are involved in the remodeling process.[3,4] It is well established that a functional lymphatic vasculature is essential for the removal of interstitial fluid as well as the maintenance of tissue homeostasis.[5,6] Moreover, studies on cutaneous lymphedema showed that chronic lymph stasis that fosters the accumulation of protein and cellular metabolites in the interstitial space coincides with increased numbers of fibroblasts and collagen deposition.[7–9] Particularly in the lung, lymphatic vessels are involved in interstitial clearance to a much greater extent than the blood capillaries and resolution of lung injury requires increased pulmonary lymph flow.[10–12]

Although remodeling of pulmonary lymphatics during pulmonary fibrosis has been recently highlighted, the underlying mechanisms, its consequences on lymphatic vessel function, as well as the impact on fibrotic changes in the lung remain to be elucidated. Therefore, we analyzed the remodeling of pulmonary lymphatics, its effect on lymphatic drainage and lung tissue homeostasis in a murine model of bleomycin-induced pulmonary fibrosis. In contrast to blood vessels, lymphatics, except for larger collecting vessels, usually lack mural cells and show only sparse basement membrane expression, allowing access of interstitial fluid into the lumen.[5] In our study we found that in fibrotic lungs an abnormal portion of lymphatic vessels exhibited mural cell coverage and excess basement membrane deposition. Noteworthy, the aberrant recruitment of mural cells to pulmonary lymphatics occurred early in the development of pulmonary fibrosis and was driven by ectopic expression of platelet-derived growth factor (PDGF-B) in lymphatic endothelial cells and signaling through platelet-derived growth factor receptor (PDGFR)-β in associated mural cells. The aberrant mural cell coverage of lymphatic vessels promoted the accumulation of macromolecular protein and hyaluronan (HA), as well as fibroblasts within the perilymphatic space, indicating a decrease in permeability and lymphatic transport. In a functional assay we were able to confirm impaired lymphatic drainage in fibrotic lungs. Importantly, inhibition of

Europe PMC Funders Author Manuscripts

PDGF-B/PDGFR-β signaling after the induction of pulmonary fibrosis prevented aberrant mural cell recruitment, as well as impaired lymphatic drainage of the lung parenchyma.

Methods

Animals

The Animal Care and Use Committee of the Bezirksregierung Düsseldorf, Germany, approved all procedures performed on mice. We used female mice at 10 to 12 weeks of age (C57Bl/6H and C57Bl/6J).

Induction of pulmonary fibrosis

For the induction of pulmonary fibrosis, mice were treated with bleomycin (Calbiochem) intraperitoneally (10 mg/kg body weight twice weekly) or intratracheally (0.05 mg). Mice treated with phosphate-buffered saline (PBS; 100 μL twice weekly) served as controls. Lungs were harvested at day 11 or 28, respectively. For histology, the animals underwent cardiac perfusion with PBS. Lungs were inflated with 4% paraformaldehyde (PFA) and then fixed in 4% (wt/vol) PFA overnight. Alternatively, lungs were inflated with Tissue-Tek OCT/PBS (1:1) and then embedded in OCT and frozen at –80°C. For isolation of RNA and proteins lungs were separated and snap-frozen in liquid nitrogen.

Inhibition of PDGFR-β signaling

PDGFR-β–inhibitor (0.5 ng) AG-1296 (Cayman Chemicals) were injected intraperitoneally 5 times per week until end point, starting 14 days after the first bleomycin injection.

488-dextran assay

488-dextran (50 μL), 10 000 MW (5 μg per 1 μL PBS; Invitrogen) were instilled intratracheally and lungs were collected at different time points after instillation. To preclude that, 488-dextran was drained via blood vessels, 50 μL of 488-dextran was injected into the tail-vein and vascular leakage was assayed.

Tumor and wound-healing studies

For a model of excisional wound healing, 8-mm circular punch biopsies on the back skin of mice were performed. Skin was analyzed at day 14 after wounding. Studies on mammary tumors were carried out on polyoma middle-T mice carrying the PyMT oncogene under the control of the murine mammary tumor virus (MMTV) long terminal repeat at age 20 weeks.

Histology, immunohistochemistry, and immunofluorescence

Sections (5 μm) were deparaffinized with xylene and rehydrated with graded ethanol. Antigen retrieval was performed by boiling the sections in low-pH citrate buffer for 15 minutes. The sections were stained and visualized by Vectastain ABC kit (Vector Laboratories). Prox1-staining was performed using the CSA-System (Dako). Primary antibodies used in this study were as follows: rabbit polyclonal to Lyve-1 at a 1:200 dilution (Abcam), anti-laminin antibody at a 1:50 dilution (Sigma-Aldrich), goat polyclonal to mouse serum albumin at a 1:500 dilution (Abcam), mouse mAb phospho-PDGFR-β at a 1:100

dilution (Cell Signaling), rabbit monoclonal antibody (mAb) PDGFR-β at a 1:100 dilution (Cell Signaling), rabbit polyclonal to PDGF BB at a 1:100 dilution (Abcam), rat anti–mouse VEGFR3 at a 1:100 dilution (BD Bioscience), human Prox1 affinity purified polyclonal AB goat immunoglobulin (Ig) G at a 1:200 dilution (R&D Systems), anti–mouse α-SMA at a 1:500 dilution (Chemicon), biotinylated hyaluronan-binding peptide at a 1:100 dilution (Calbiochem), D2-40 and S100A4 (FSP) at a 1:200 dilution (Dako). The fluorochromeconjugated Alexa 488, Alexa 568, and streptavidin 488 (Invitrogen) were used as secondary antibodies.

Quantitative analysis of histology markers

For quantitative analysis of immunohistochemical markers, sections were photographed into JPEG images at 21°C, at a magnification of 200, and with a numeric apature of 0.50 using a Nikon Eclipse E1000 microscope and the Nikon DS-Ri1 camera system. The area (no. of pixels) marked by each marker was measured using ImageJ 1.42 software (National Institute of Health; NIH) and calculated as the percentage of the area covered by DAPI. For quantitative analysis of lymphatic vessel density and mural cells coverage, vessels per field were counted. Mural cells coverage was calculated as percentage of total number of lymphatic vessels.

Isolation of murine lymphatic endothelial cells

For lymphatic endothelial cells (LEC)–isolation animals underwent cardiac perfusion with PBS-ethylenediaminetetraacetic acid (EDTA; 5mM). Lungs were inflated with 1 mL collagenase type 3 (Worthington), scrambled, and then digested in collagenase type 3 (Worthington) for 30 minutes at 37°C. After washing and counting, cells were resuspended in MACS-buffer according to the manufacturers' instructions (Miltenyi Biotec) and incubated with Lyve-1 antibody at a 1:100 dilution (Abcam). LECs were again washed, resuspended in MACS-buffer and incubated with anti–rabbit IgG microbeads (Miltenyi Biotec) with 20 μL per 10^7 cells. Cells were then separated by MACS-seperator (Miltenyi Biotec), counted and plated on gelatin-covered 6-well plates at a density of 7×10^5 cells per well and incubated for 12 hours in Clonetics endothelial cell basal medium-2 (Lonza) supplemented with Clonetics EGM-2 MV SingleQuots (Lonza). LECs were isolated from bleomycin-treated (intraperitoneally 10 mg/kg body weight twice weekly) and PBS-treated (intraperitoneally 100 μL per mouse twice weekly) mice. For ex vivo studies LECs were isolated from untreated adult mice, plated, and subsequently treated with bleomycin (10 μg/mL) for 12 hours. After isolation of LECs, cells were plated onto glass coverslips (150 000 cells/12 mm coverslips placed in wells from 24-well plates) that were previously coated with 10 μg/mL fibronectin (Sigma-Aldrich) and collagen 1 (BD Bioscience) in 0.1% gelatin in PBS and placed into 37°C for 1 hour to determine their lymphatic identity (supplemental Figure 4, available on the *Blood* Web site; see the Supplemental Materials link at the top of the online article). After leaving cells to attach overnight at 37°C, 5% CO_2 they were fixed with 4% PFA in PBS for 10 minutes at room temperature. Cells were washed with 1× PBS and permeabilized with 0.1% Triton X-100 (Fluka) in PBS. They were blocked with 1% bovine serum albumin (BSA)–PBS at room temperature. Then antibodies were added. Primary antibodies were used as follows: Prox1 (R&D), and Lyve-1 (Abcam) all at a 1:200 dilution. Secondary antibodies were Alexa 488 and Alexa 568 (Invitrogen). DAPI

(Invitrogen) was used to stain for cell nuclei at a 1:500 dilution. Coverslips were mounted with mouting medium (Dako).

RNA preparation and real-time PCR

Total RNA was isolated by the phenol/chloroform extraction method. RNA (1 μg) was reverse-transcribed into cDNA. For PCR reactions, TaqMan universal mastermix (Applied Biosystems) was used. Primer sequences for qualitative and quantitative PCR: 16S: F 5′-AGATGATCGAGCCGCGC-3′ R 5′-GCTACCAGGGCCTTTGAGATGGA-3′ VEGF-D: F 5′-CCGAGCAGCTTCTAGTTTGGA-3′ R 5′-ATGGGATGCTGAGCGTGAGT-3′; Murine PDGFR-beta: F 5′-TTGCCAGTTCCACCTTGAATG-3′ R 5′-TTGTGCCTCAGGCTCTGCTT-3′; Murine PDGF-B: F 5′-CATCCGCTCCTTTGATGATCTT-3′ R 5′-ATGAGCTTTCCAACTCGACTCC-3′; Murine Ephrin B2: F 5′-GACTTCGGAGCTTGCACCATC-3′ R 5′-AACACCCGAATCCATAGACGGTAA-3′; Murine Ephrin B4: F 5′-CGTCCTGATGTCACCTATACCTTTGAGG-3′ R 5′-GAGTACTCAACTTCCCTCCCATTGGTCT-3′; Murine Endoglin: F 5′-CTGCCAATGCTGTGCGTGAA-3′ R 5′-GCTGGAGTCGTAGGCCAAGT-3′; Murine ANG:1 F 5′-GATCTTACACGGTGCCGATT-3′ R 5′-TTAGATTGGAAGGGCCACAG-3′ (118 bp); Murine ANG2 F 5′-TCCAAGAGCTCGGTTGCTAT-3′ R 5′-AGTTGGGGAAGGTCAGT-GTG-3′ (114 bp). For semiquantitative analysis, a 2% agarose gel was loaded with the PCR-product and ran for 40 minutes at 80 volts. Agarose gel was scanned with the Benchtop UV Transilluminator (UVP). Integrated density was determined using ImageJ 1.42 software (NIH) and normalized to ribosomal protein (16s). cDNA standards for real-time PCR were prepared according to the standard procedures. The amount of standard cDNA was determined photometrically. The standard concentrations ranged from 100 to 0.001 fg/μL. Quantification was done in a 2-step real-time PCR with a denaturation step at 95°C for 10 minutes, followed by 40 cycles at 95°C for 15 seconds and at 60°C for 1 minute.

Western blot analysis

One entire lung lobe was homogenized in lysis buffer, and Western blotting was performed according to standard procedures. The following antibodies were used: mouse mAb phospho–PDGFR-β (Cell Signaling) and rabbit mAb PDGFR-β (Cell Signaling). For quantitative analysis, the membranes were scanned with the Fusion-FX7 (Vilber Lourmat) and integrated density was determined using ImageJ software (NIH).

HA-isolation

Frozen lungs were lyophilized and dry weight was determined. Crushed lungs were transferred in pronase-buffer (protease 6 mg/mL from *Streptomyces griseus*; Sigma-Aldrich in 100mM Tris HCl and 1mM $CaCl_2$) at 60°C for 24 hours. HA was precipitated with a 3-fold volume of absolute ethanol and the pellet was resuspended in 150 μL aqua dest. Probes were diluted 1:50 and hyaluronic acid was determined by a sandwich protein binding assay from Corgenix (HA test kit; Corgenix).

Bone marrow transplantation and in vivo neutralization of Lyve-1

CD44 knockout mice and corresponding wild-type (WT) mice (C57JBl/6J) served as bone marrow (BM) donors. C57Jl/6J mice were used as recipients. Isolation of BM: hindlimbs were removed and cleaned. Both tops of the femur were cut off and the bones were flushed with each 5 mL RPMI 1640 + 2% FBS + 10 units/mL heparin + penicillin and streptomycin. The solution was put through a sterile 40 μm nylon Cell Strainer (Falcon). Cells were washed twice, counted, and resuspended in RPMI 1640 + 10 units/mL heparin + penicillin and streptomycin with 5×10^6 cells per 100 μL medium. Cells were injected right after isolation.

Treatment of the recipients: 1 week before and 2 weeks after irradiation mice were given acidified, antibiotic water. Water (250 mL) was adjusted to a pH of 2.6 with concentrated HCL. Neomycin (10 mg/mL; Sigma-Aldrich) and 25 mg/mL Polymyxin B (Sigma-Aldrich) was added. Recipient mice were irradiated with 10 gray. After 24 hours at the latest 5×10^6 BM cells were injected into the tail vein. Three weeks after irradiation treatment with bleomycin was started as previously described.

To neutralize LYVE-1, 100 μg of anti–LYVE-1 (R&D Systems) were injected intraperitoneally every other day, starting at day 15 after the first bleomycin. Lungs were harvested at day 28.

Human lung specimens

Human lung tissue samples from non-IPF and IPF patients were analyzed. Non-IPF specimens were obtained at the time of surgery for a localized lung tumor from an uninvolved segment. IPF samples were obtained at the time of surgical lung biopsy or transplantation. The recruitment of PDGFR-β–positive mural cells to D2-40–positive lymphatic vessels was assessed by 2 independent observers.

Statistical analysis

Statistical analysis was done using Prism 4.0 software (GraphPad). Statistical significance was determined by an unpaired Student *t* test.

Results

Aberrant mural cell recruitment to pulmonary lymphatics and perilymphatic formation of fibrosis

To analyze the remodeling of lymphatics during pulmonary fibrosis and its effect on homeostasis of the lung parenchyma, we treated mice with bleomycin (10 mg/kg body weight, twice per week intraperitoneally) for up to 28 days, which induced profound fibrotic changes in the lung (supplemental Figure 1A).[13] First, we noticed that fibrotic lesions initially develop around vascular structures that are negative for the blood vessels marker CD 34 but express the lymphatic marker Lyve-1 (supplemental Figure 1B). Therefore, we conducted a structural comparison of Lyve-1–positive vessels in lungs from healthy control and bleomycin-treated mice with different degrees of fibrosis (Figure 1A). In contrast to blood vessels, lymphatics, except for larger collecting vessels, usually lack mural cells and a

basement membrane.[14] Consistent with this, only a few lymphatic vessels in control lungs showed sparse association with mural cells as evaluated by double-immunofluorescence for lymphatic marker Lyve-1 and α-smooth muscle actin (SMA). However, in fibrotic lungs approximately 65% of Lyve-1–positive vessels showed ectopic mural cell coverage (Figure 1A-B). Although, Lyve-1 is usually a reliable marker for lymphatic vessels in most tissues, it has been reported that a subset of pulmonary venous vessels expresses Lyve-1.[15] Therefore, we performed an analysis with 2 of the most specific lymphatic markers vascular endothelial growth factor receptor 3 (VEGFR3) and PROX-1 to determine the identity of those Lyve-1–positive vessels in the lung. Indeed, whereas nearly all the VEGFR3-positive and PROX-1–positive vessels coexpressed Lyve-1 (supplemental Figure 1C-D,G,H), only approximately 70% of Lyve-1–expressing vessels were positive for VEGFR3 and PROX-1 (supplemental Figure 1E-H). However, when we assessed association of mural cells and pulmonary lymphatics by doubleimmunofluorescence for VEGFR3 and SMA, again nearly 75% of lymphatics in fibrotic lungs showed ectopic mural cell coverage (Figure 1C, supplemental Figure 2A). Similar results were obtained when mural cell coverage was evaluated by double labeling for PROX-1 and SMA (Figure 1D, supplemental Figure 2B), clearly showing that pulmonary lymphatics recruit SMA-expressing mural cells during the development of pulmonary fibrosis. Noteworthy, even in specimen with early histopathologic signs of fibrosis, aberrant association between lymphatic endothelial cells and mural cells was present (Figure 1A), indicating that this event occurs early during the pathogenesis of pulmonary fibrosis. Furthermore, lymphatic vessels in fibrotic lungs showed excessive basement membrane deposition as determined by simultaneous detection of VEGFR3 and the basement membrane marker laminin (supplemental Figure 2C). Importantly, a quantitative analysis of lymphatic vessel density using VEGFR3 and PROX-1 at day 28 revealed no significant differences in the number of lymphatic vessels in fibrotic lungs compared with lungs from PBS-treated control animals (supplemental Figure 2D-E). Next, we tested whether aberrant mural cell recruitment to lymphatic vessels occurs in other pathologies that involve remodeling of the lymphatic vasculature. The analysis of mammary tumors and healing cutaneous wounds in mice revealed no mural cell coverage of lymphatic vessels (supplemental Figure 3A). However, induction of pulmonary fibrosis by the alternative route of intratracheal bleomycin application again resulted in association of lymphatics and mural cells (supplemental Figure 3B), indicating that aberrant recruitment of mural cells is specific to the pathogenesis of pulmonary fibrosis. To determine the onset of mural cell recruitment during pulmonary fibrosis, we analyzed lung specimen from bleomycin-treated mice at different time points. We found that aberrant mural cell recruitment to pulmonary lymphatics occurs around day 11 after the first bleomycin treatment (supplemental Figure 3C). Noteworthy, at this time point, no histopathologic signs of fibrosis were detectable. This result argues that the abnormal recruitment of mural cells to pulmonary lymphatics represents an early pathophysiologic event during the formation of fibrotic lesions.

PDGF-B/PDGFR-β signaling is involved in aberrant mural cell recruitment

To identify potential signaling pathways that mediate aberrant mural cell recruitment in pulmonary fibrosis, we performed gene expression analysis on whole lung lysates including various factors that are known to be involved in the recruitment of mural cells to blood

vessels and/or lymphatic vessels (supplemental Figure 3D-K).[5,16–18] Among the potential targets, *pdgf-b* and its cognate receptor *pdgfr*-β (encoded by the gene *pdgfrb*) showed increased expression in lungs from bleomycin-treated mice (supplemental Figure 3A-F). The PDGF-B/PDGFR-β signaling axis is known to be essential for the recruitment of mural cells to blood capillaries.[17,19] Next, we checked *pdgf-b* expression levels in isolated lymphatic endothelial cells from control lungs and bleomycin-treated lungs. As shown in Figure 2A, the expression levels of *pdgf-b* in LECs from healthy lungs are very low, whereas lymphatic endothelial cells from fibrotic lungs show a strong increase in *pdgf-b* expression. In addition, ex vivo treatment of LECs from healthy lungs with bleomycin leads to augmented *pdgf-b* expression (supplemental Figure 3L). Furthermore, we found that lymphatic vessels show intense immunostaining for PDGF-B only in fibrotic lungs and that associated mural cells express the corresponding receptor PDGFR-β (Figure 2B-C). This observation strongly argues that ectopic expression of PDGF-B pulmonary lymphatics is involved in aberrant mural cell recruitment. We next wished to determine whether the ectopic expression of PDGF-B in lymphatic vessels results in active PDGF-B/PDGFR-β signaling in fibrotic lungs. By probing whole lung protein lysates with an antibody specific for the phosphorylated form of PDGFR-β, followed by an anti–PDGFR-β antibody by Western blotting, we were able to quantify the amount of phosphorylated and therefore activated PDGFR-β relative to total PDGFR-β (Figure 2D-E). As shown in Figure 2E, lungs from bleomycin-treated mice show a dramatic increase in the ratio of phosphorylated PDGFR-β to total PDGFR-β, whereas healthy lungs only show very modest receptor activation. Importantly, activation of PDGFR-β in mural cells that are aberrantly associated with lymphatic vessels can only be detected in fibrotic lungs and not in healthy lungs (Figure 2F), suggesting that an active PDGF-B/PDGFR-β signaling axis between LECs and mural cells drives the process of aberrant lymphatic patterning in pulmonary fibrosis.

Next, we investigated whether the inhibition of the PDGF-B/PDGFR-β signaling axis has an impact on aberrant mural cell recruitment by administration of the PDGFR-β–inhibitor AG-1296[20] (0.5 ng per mouse, 5 times per week intraperitoneally) at the onset of abnormal mural cell recruitment. Consistent with our hypothesis, inhibition of PDGF-B/PDGFR-β signaling starting at day 14 after the first bleomycin treatment resulted in a significant reduction of pulmonary lymphatics with ectopic mural cell coverage (Figures 2G-I, supplemental Figure 5A).

Accumulation of fibrogenic molecules and fibroblasts in the perilymphatic space

The lymphatic vasculature is essential for the removal of interstitial fluid and the maintenance of tissue homeostasis.[6,21] Consequently, impaired lymphatic transport will foster the accumulation of substances that are subject to continuous lymphatic drainage, such as macromolecular protein albumin and the glycosaminoglycan HA.[6,7] Of note, it has been shown that albumin-bound substances like lysophosphatidic acid are major signaling molecules in pulmonary fibrosis.[22] In addition, HA is capable of supporting proliferation, migration, and differentiation of fibroblasts and has been shown to contribute to an invasive fibroblast phenotype during pulmonary fibrosis.[23–27] Therefore, we investigated whether excessive basement membrane deposition and ectopic mural cell coverage of pulmonary lymphatic vessels affect lymphatic drainage of the lung parenchyma and the accumulation of

those fibrogenic substances. We found that perilymphatic accumulation of albumin (supplemental Figure 5B) as well as HA (Figure 3A), which are low abundant in healthy lungs, occurs already in early fibrotic lesions and then further progresses along with the development of fibrotic foci, indicating impaired clearance of these substances by the lymphatic vasculature. Consistent with this and analogous to the accumulation pattern for albumin and HA, we observed perilymphatic aggregation of fibroblasts expressing fibroblast-specific protein-1 (FSP; Figure 3C-D). Importantly, this occurred even in specimen with very modest histopathologic signs of pulmonary fibrosis and along with the progression of fibrotic foci the number of perilymphatic fibroblasts further increased (Figure 3C). These observations suggest that chronic lymph stasis because of PDGF-B–driven mural cell recruitment and impaired drainage capacity of pulmonary lymphatics trigger the accumulation of fibroblasts and contribute to pulmonary fibrosis. Consistent with this, we found that disruption of PDGF-B/PDGFR-β signaling reduced perilymphatic accumulation of albumin and HA (supplemental Figure 5B; Figure 3A) as well as overall pulmonary HA content (Figure 3B), indicating improved lymphatic clearance of the lung parenchyma. Consequently, inhibition of aberrant mural cell recruitment by AG-1296 also prevented the subsequent aggregation of fibroblasts in the perilymphatic space (Figure 3C-D).

Various HA surface receptors contribute to HA clearance in the lung with different outcomes on pulmonary fibrosis

HA can be pathogenic in pulmonary fibrosis and Lyve-1 as well as CD44 are known HA cell surface receptors.[28,29] Therefore, we aimed to further investigate the role of these receptors in HA-clearance in the setting of pulmonary fibrosis. Bleomycin treatment per se did not augment circulating HA levels (Figure 4G). Interestingly, in vivo neutralization of Lyve-1 by administration of a blocking antibody during bleomycin treatment largely augmented plasma HA-levels but had no effect on lung tissue HA levels (Figure 4G-H). However, blocking Lyve-1 further increased the number of perilymphatic fibroblasts and aggravated pulmonary fibrosis (Figure 4A-C). This result is rather surprising with regard to the fact that Lyve-1–deficient mice show unaltered plasma HA levels and indicate that Lyve-1 is involved in HA-clearance on bleomycin challenge. Immunostaining of CD44 and MAC2 revealed expression of CD44 on macrophages in lungs of bleomycin treated mice (Figure 4D). To further evaluate the role of CD44 expressed on myeloid cells for HA-clearance in the context of pulmonary fibrosis, we transferred CD44-deficient and WT BM into lethally irradiated C57Bl6/J mice before bleomycin treatment as suggested by the reviewers. In contrast to blocking Lyve-1, mice that were reconstituted with CD44-deficient BM had unchanged circulating HA levels on bleomycin treatment compared with animals reconstituted with WT BM (Figure 4G). Of note a reduction in pulmonary HA content and a reduction in perilymphatic fibroblasts was detected (Figure 4F-H). However this did not translate into a significant overall amelioration of pulmonary fibrosis in these animals (Figure 4E).

Impaired lymphatic drainage during pulmonary fibrosis is rescued by the inhibition of PDGF-B/PDGFR-β signaling

Finally, we analyzed permeability and transport capacity of pulmonary lymphatics in a functional assay based on 488-dextran clearance from the lungs of healthy and fibrotic mice. After intratracheal instillation of the high molecular weight fluorescent dye 488-dextran and

even distribution across the lung for 15 minutes, we measured the clearance of 488-dextran from the lung to pretracheal lymph nodes. As depicted in Figure 5A-B, in control mice, 488-dextran was almost completely removed from the lung and drained to pretracheal lymph nodes (LNs) after 50 minutes. However, in fibrotic lungs from bleomycin-treated mice, drainage to LNs was impaired, resulting in the accumulation of 488-dextran in the lung parenchyma. Importantly, inhibition of the PDGF-B/PDGFR-β signaling axis at the onset of aberrant mural cell recruitment restored the clearance of 488-dextran from the lung to pretracheal LNs and ameliorated pulmonary fibrosis (Figure 5A-B). Noteworthy, increased permeability of pulmonary blood vessels at the time point of examination as an alternative explanation for the accumulation of macromolecular protein and HA was excluded by intravenous injection of 488-dextran and subsequent evaluation for capillary leakage on lung sections, which did not show any differences between control lungs and fibrotic lungs (supplemental Figure 5C).

Aberrant mural cell recruitment in human IPF lungs

We have analyzed human lung tissue samples from non-IPF and IPF patients. Non-IPF specimens were obtained at the time of surgery for a localized lung tumor from an uninvolved segment. IPF samples were obtained at the time of surgical lung biopsy or transplantation. As shown in Figure 6, pulmonary lymphatics from IPF patients show an increase in associated mural cells compared with non-IPF patients (25.36 ± 3.065 and 6.900 ± 1.735, respectively) as visualized by double-immunofluorescence for D2-40 and PDGFR-β. Interestingly, the overall degree of mural cell coverage is lower than in the murine model of pulmonary fibrosis (25.36 ± 3.065 for IPF and 6.900 ± 1.735 for non-IPF samples vs 65.55 ± 4.776 for bleomycin-treated mice and 27.11 ± 9.085 for control mice). However, unlike in the murine model, we observe an overall increase in the number of lymphatic vessels in human fibrotic lungs, indicating neoformation of lymphatic vessels during pulmonary fibrosis.

Taken together, our results indicate that aberrant mural cell recruitment to the lymphatic vasculature driven by PDGF-B/PDGFR-β signaling represents a previously unidentified pathogenetic event in pulmonary fibrosis and identify the lymphatic drainage capacity as a critical mediator of this fibroproliferative process. We propose that impaired lymphatic transport plays a role in the formation of fibrotic lesions in the lung, and that restoring lymphatic drainage of the lung parenchyma has the potential to ameliorate pulmonary fibrosis.

Discussion

To assess the role of the lymphatic vasculature for the pathogenesis of pulmonary fibrosis, we have analyzed lymphatic vessels in healthy control lungs and fibrotic lungs in a murine model of pulmonary fibrosis. We found that in fibrotic lungs a large number of lymphatic vessels show aberrant association with mural cells and excessive basement membrane deposition.

The specificity of markers to identify lymphatic vessels, particularly in the lung has been a matter of debate. It has been reported that Lyve-1 is also expressed on a subset of pulmonary

blood vessels,[15] and indeed, only approximately 70% of Lyve-1–positive vessels show coexpression of other lymphatic markers like VEGFR-3 and Prox-1, further indicating that Lyve-1–expression in the lung comprises nonlymphatic vessels. However, when we used VEGFR-3 or Prox-1 as markers, we still observed approximately 75% of pulmonary lymphatics with ectopic mural cell coverage in fibrotic lungs, showing that indeed lymphatic vessels are involved in the perivascular formation of fibrotic lesions after bleomycin challenge.

Although remodeling of pulmonary lymphatics during pulmonary fibrosis has been recently reported, the impact of the lymphatic vasculature on fibroproliferative changes in the lung remains a matter of debate.[3,30] In contrast to blood vessels, lymphatic capillaries lack mural cells and a basement membrane. This characteristic structural feature of lymphatics allows facilitated access of interstitial fluid to the vessel lumen and is therefore essential for the drainage function of lymphatic vessels.[5] Here, we report for the first time an abnormal proportion of lymphatic vessels covered with mural cells and impaired lymphatic drainage during pulmonary fibrosis. The phenomenon of aberrant mural cell recruitment to lymphatic vessels with diminished tissue drainage has so far only been described in hereditary cutaneous lymphedema distichiasis.[5] Interestingly, in other studies on cutaneous lymphedema it has been reported that chronic lymph stasis coincides with increased fibroblasts numbers and collagen deposition in the skin but the mechanisms that link those 2 observations remained largely unexplored.[8,9,31–33] Interestingly, we observe perilymphatic accumulation of fibroblasts in the lungs of bleomycin-treated mice and show that aberrant mural cell recruitment to pulmonary lymphatics with subsequent lymph stasis is an early event in the development of pulmonary fibrosis. Therefore, impaired lymphatic drainage in the lung with accumulation of fibrogenic signaling molecules probably contributes to the aggregation of fibroblasts in the perilymphatic space.

Although, it has been reported that IPF involves an increase in the number of lymphatic vessels,[3] the question whether lymphangiogenesis occurs during pulmonary fibrosis remains a matter of debate.[4] Importantly, our quantitative analysis of lymphatic vessel density using the 2 most reliable lymphatic markers VEGFR3 and PROX-1 revealed no significant differences in the number of lymphatic vessels in fibrotic lungs compared with lungs from PBS-treated control animals. However, unlike in the murine model, we observe an overall increase in the number of D2-40–positive lymphatic vessels in human fibrotic lungs, indicating neoformation of lymphatic vessels.

We show that during pulmonary fibrosis, albumin and HA progressively accumulate in the perilymphatic and interstitial space. Lysophosphatidic acid, which is bound to albumin, has been shown to be a major fibroblast chemoattractant in pulmonary fibrosis.[22] In addition, it is known that HA can trigger the proliferation, migration, and differentiation of fibroblasts in vitro and recently, it has been demonstrated in vivo that HA induces an aggressive fibroblast phenotype and severe pulmonary fibrosis.[23–27] Therefore, the accumulation of those fibrogenic molecules because of impaired lymphatic clearance could trigger the perilymphatic formation of fibrotic lesions. Consistent with this, we observe accumulation of fibroblasts in the perilymphatic space. An alternative explanation for the interstitial accumulation of lysophosphatidic acid and HA could be increased leakage of blood

capillaries because of bleomycin treatment. However, assessment of vascular permeability by 488-dextran injection showed no difference between lungs from control mice and bleomycin-treated mice.

The current data indicate that LYVE-1 is involved in HA clearance in this model of lung fibrosis. In unchallenged Lyve-1–deficient mice HA concentrations were not affected.[28] Furthermore blocking of LYVE increased recruitment of FSP-1 positive fibroblasts to the lymphatics and increased overall lung fibrosis. These findings are in line with our current working hypothesis that stabilization and disturbed function of lympathic vessels aggravates lung fibrosis. This could explain why we did not see an effect of blocking LYVE-1 on total HA content of lungs at the end of the experimental period when lymphatic vessel function was impaired by increased fibroblast recruitment. Furthermore staining of HA and determination of HA plasma concentrations are based on HA-binding protein dependent assays that do not allow the detection of small HA. Therefore it is possible that small HA concentrations are increased after blocking of LYVE-1 and that small HA-mediated signaling in turn contributes to the detrimental effects of blockin Lyve-1.[34] The role of CD44 on hematopoetic cells (eg, macrophages) is probably different from Lyve-1 because CD44 is not involved in the clearance of HA but rather in a biologic response, such as signaling or adhesion of inflammatory cells to HA-rich matrices.[35] The transfer of CD44-deficient BM clearly showed that CD44 on hematopoetic cells augments HA content of the fibrotic lungs but has no effect of HA clearance. It is conceivable that CD44 on monocytes/macrophages is involved in the recruitment of macrophages to the HA-rich matrix structures, such as HA-cables in the fibrotic lungs.[35,36] In turn, secretion of cytokines and growth factors, such as PDGF[37,38] and IL-1, by these macrophages may induce further HA-synthesis and stimulate recruitment of FSP-1–positive fibroblasts.[39] In addition, small HA may via CD44 contribute to macrophage activation.[34] This conclusion is supported by the reduced HA-content and reduced fibroblastic response after transfer of CD44-deficient BM. All together our results point toward differential role of Lyve-1 and CD44. Lyve-1 may be involved in pulmonary HA-clearance on bleomycin challenge and is rather protective in the context of pulmonary fibrosis. In contrast CD44 on hematopoetic cells may play an important role in regulating HA synthesis and recruitment of macrophages to HA-rich areas.

After entry of fluid into the initial lymphatics, the fluid transport within lymphatic vessels also depends on intermittent and reciprocal pressure changes within the lung tissue und the thorax because of alternating expansion and retraction during respiration.[6] Therefore, in addition to impaired entry of interstitial fluid and macromolecules into initial lymphatics because of aberrant mural cell recruitment and excessive basement membrane deposition, the reduced expansivity of fibrotic lungs could further aggravate impaired lymphatic drainage of the lung parenchyma.

Although, PDGF-B/PDGFR-β signaling has been shown to be involved in pulmonary fibrosis (eg, by driving fibroblast proliferation),[40,41] we demonstrate that the aberrant recruitment of mural cells to pulmonary lymphatics is driven by ectopic PDGF-B expression in LECs and signaling through PDGFR-β in associated mural cells.

Consequently, inhibition of mural cell recruitment by AG-1296 maintained lymphatic drainage of the lung parenchyma and prevented the subsequent aggregation of fibroblasts in the perilymphatic space. Although, potential off-targets of tyrosine kinase-inhibiting compounds have been a matter of debate, AG-1296 has been shown to be a very potent inhibitor with high specifity for the PDGF-receptors and minimal off-target effects in the kinome.[42] Importantly, in hereditary cutaneous lymphedema distichiasis, dermal lymphatics with aberrant mural cell coverage also show ectopic expression of PDGF-B,[5] further emphasizing the idea that increased PDGF-B expression in LECs can drive atypical patterning of the lymphatic vasculature and subsequent lymph stasis. Previous studies suggested that inhibition of PDGF-B/PDGFR-β signaling before the induction of fibrosis can ameliorate fibrosis in mouse models by preventing fibroblast proliferation/migration directly.[40,41] Importantly, however, our approach in this study aims at preventing aberrant mural cell recruitment to pulmonary lymphatics and impaired lymphatic drainage in the lung, 2 previously unanticipated pathogenetic events in pulmonary fibrosis. The question whether ectopic PDGF-B expression by LECs has direct effects on fibroblast proliferation/migration will have to be examined in further studies.

Many studies prevent pulmonary fibrosis by prophylactic blocking of profibrotic pathways, either by genetic ablation of signaling components or administration of antifibrotic treatment before the induction of fibrosis but fail to resolve pulmonary fibrosis in a therapeutic study design.[40,41] However, we would like to point out that our approach ameliorates pulmonary fibrosis in a therapeutic setting. Along with this, a recent clinical trial has shown that inhibiting tyrosine kinase receptors including PDGFR-β is efficient in ameliorating IPF symptoms and preserving quality of life.[43]

Taken together, we identified aberrant mural cell recruitment to pulmonary lymphatics as a novel and critical event in the progression of pulmonary fibrosis. Furthermore, our observations argue that a critical mediator of fibroproliferative changes in the lung lies in the drainage capacity of pulmonary lymphatics. Finally, these findings provide new insights into pathogenesis of pulmonary fibrosis and might also open new therapeutic avenues for the treatment of disorders that involve tissue fibrosis.

Supplementary Material

Refer to Web version on PubMed Central for supplementary material.

Acknowledgments

The authors acknowledge the financial support from the Interne Forechungsförderung Essen (IFORES) program of the University Hospital Essen and the Deutsche Forschungsgemeinschaft to A.K.M. and C.S. (STO/787 3-1), respectively.

References

1. Olson AL, Swigris JJ, Lezotte DC, Norris JM, Wilson CG, Brown KK. Mortality from pulmonary fibrosis increased in the United States from 1992 to 2003. Am J Respir Crit Care Med. 2007; 176(3):277–284. [PubMed: 17478620]
2. Selman M, Pardo A. Role of epithelial cells in idiopathic pulmonary fibrosis: from innocent targets to serial killers. Proc Am Thorac Soc. 2006; 3(4):364–372. [PubMed: 16738202]

3. El-Chemaly S, Malide D, Zudaire E, et al. Abnormal lymphangiogenesis in idiopathic pulmonary fibrosis with insights into cellular and molecular mechanisms. Proc Natl Acad Sci U S A. 2009; 106(10):3958–3963. [PubMed: 19237567]
4. Ebina M, Shibata N, Ohta H, et al. The disappearance of subpleural and interlobular lymphatics in idiopathic pulmonary fibrosis. Lymphat Res Biol. 2010; 8(4):199–207. [PubMed: 21190492]
5. Petrova TV, Karpanen T, Norrmen C, et al. Defective valves and abnormal mural cell recruitment underlie lymphatic vascular failure in lymphedema distichiasis. Nat Med. 2004; 10(9):974–981. [PubMed: 15322537]
6. Aukland K, Reed RK. Interstitial-lymphatic mechanisms in the control of extracellular fluid volume. Physiol Rev. 1993; 73(1):1–78. [PubMed: 8419962]
7. Reed RK, Laurent TC, Taylor AE. Hyaluronan in prenodal lymph from skin: changes with lymph flow. Am J Physiol. 1990; 259(4 Pt 2):H1097–H1100. [PubMed: 2221117]
8. Schirger A, Harrison EG Jr, Janes JM. Idiopathic lymphedema. Review of 131 cases. JAMA. 1962; 182:14–22. [PubMed: 14498461]
9. Rockson SG. Lymphedema. Am J Med. 2001; 110(4):288–295. [PubMed: 11239847]
10. Wagner EM, Blosser S, Mitzner W. Bronchial vascular contribution to lung lymph flow. J Appl Physiol. 1998; 85(6):2190–2195. [PubMed: 9843542]
11. Traber DL, Lentz CW, Traber LD, Herndon DN. Lymph and blood flow responses in central airways. Am Rev Respir Dis. 1992; 146(5 Pt 2):S15–S18. [PubMed: 1443899]
12. Lauweryns JM, Baert JH. Alveolar clearance and the role of the pulmonary lymphatics. Am Rev Respir Dis. 1977; 115(4):625–683. [PubMed: 322558]
13. Stockmann C, Kerdiles Y, Nomaksteinsky M, et al. Loss of myeloid cell-derived vascular endothelial growth factor accelerates fibrosis. Proc Natl Acad Sci U S A. 2010; 107(9):4329–4334. [PubMed: 20142499]
14. Oliver G, Alitalo K. The lymphatic vasculature: recent progress and paradigms. Annu Rev Cell Dev Biol. 2005; 21:457–483. [PubMed: 16212503]
15. Gordon EJ, Gale NW, Harvey NL. Expression of the hyaluronan receptor LYVE-1 is not restricted to the lymphatic vasculature; LYVE-1 is also expressed on embryonic blood vessels. Dev Dyn. 2008; 237(7):1901–1909. [PubMed: 18570254]
16. Foo SS, Turner CJ, Adams S, et al. Ephrin-B2 controls cell motility and adhesion during blood-vessel-wall assembly. Cell. 2006; 124(1):161–173. [PubMed: 16413489]
17. Hellström M, Kalen M, Lindahl P, Abramsson A, Betsholtz C. Role of PDGF-B and PDGFR-beta in recruitment of vascular smooth muscle cells and pericytes during embryonic blood vessel formation in the mouse. Development. 1999; 126(14):3047–3055. [PubMed: 10375497]
18. Shimoda H, Bernas MJ, Witte MH, Gale NW, Yancopoulos GD, Kato S. Abnormal recruitment of periendothelial cells to lymphatic capillaries in digestive organs of angiopoietin-2-deficient mice. Cell Tissue Res. 2007; 328(2):329–337. [PubMed: 17235601]
19. Lindahl P, Johansson BR, Leveen P, Betsholtz C. Pericyte loss and microaneurysm formation in PDGF-B-deficient mice. Science. 1997; 277(5323):242–245. [PubMed: 9211853]
20. Kovalenko M, Ronnstrand L, Heldin CH, et al. Phosphorylation site-specific inhibition of platelet-derived growth factor beta-receptor autophos-phorylation by the receptor blocking tyrphostin AG1296. Biochemistry. 1997; 36(21):6260–6269. [PubMed: 9174341]
21. Dumont DJ, Jussila L, Taipale J, et al. Cardiovascular failure in mouse embryos deficient in VEGF receptor-3. Science. 1998; 282(5390):946–949. [PubMed: 9794766]
22. Tager AM, LaCamera P, Shea BS, et al. The lyso-phosphatidic acid receptor LPA1 links pulmonary fibrosis to lung injury by mediating fibroblast recruitment and vascular leak. Nat Med. 2008; 14(1):45–54. [PubMed: 18066075]
23. Webber J, Jenkins RH, Meran S, Phillips A, Steadman R. Modulation of TGFbeta1-dependent myofibroblast differentiation by hyaluronan. Am J Pathol. 2009; 175(1):148–160. [PubMed: 19541937]
24. Webber J, Meran S, Steadman R, Phillips A. Hyaluronan orchestrates transforming growth factor-beta1-dependent maintenance of myofibroblast phenotype. J Biol Chem. 2009; 284(14):9083–9092. [PubMed: 19193641]

25. Meran S, Thomas D, Stephens P, et al. Involvement of hyaluronan in regulation of fibroblast phenotype. J Biol Chem. 2007; 282(35):25687–25697. [PubMed: 17611197]
26. Meran S, Thomas DW, Stephens P, et al. Hyaluronan facilitates transforming growth factor-beta1-mediated fibroblast proliferation. J Biol Chem. 2008; 283(10):6530–6545. [PubMed: 18174158]
27. Li Y, Jiang D, Liang J, et al. Severe lung fibrosis requires an invasive fibroblast phenotype regulated by hyaluronan and CD44. J Exp Med. 2011; 208(7):1459–1471. [PubMed: 21708929]
28. Gale NW, Prevo R, Espinosa J, et al. Normal lymphatic development and function in mice deficient for the lymphatic hyaluronan receptor LYVE-1. Mol Cell Biol. 2007; 27(2):595–604. [PubMed: 17101772]
29. Teder P, Vandivier RW, Jiang D, et al. Resolution of lung inflammation by CD44. Science. 2002; 296(5565):155–158. [PubMed: 11935029]
30. Ebina M, Shimizukawa M, Shibata N, et al. Heterogeneous increase in CD34-positive alveolar capillaries in idiopathic pulmonary fibrosis. Am J Respir Crit Care Med. 2004; 169(11):1203–1208. [PubMed: 14754760]
31. Ryan TJ, De Berker D. The interstitium, the connective tissue environment of the lymphatic, and angiogenesis in human skin. Clin Dermatol. 1995; 13(5):451–458. [PubMed: 8665456]
32. Piller NB. Lymphoedema, macrophages and benzopyrones. Lymphology. 1980; 13(3):109–119. [PubMed: 6255262]
33. Piller NB. Macrophage and tissue changes in the developmental phases of secondary lymphoedema and during conservative therapy with benzopyrone. Arch Histol Cytol. 1990; 53(Suppl):209–218. [PubMed: 2252630]
34. McKee CM, Penno MB, Cowman M, et al. Hyaluronan (HA) fragments induce chemokine gene expression in alveolar macrophages. The role of HA size and CD44. J Clin Invest. 1996; 98(10):2403–2413. [PubMed: 8941660]
35. Lauer ME, Erzurum SC, Mukhopadhyay D, et al. Differentiated murine airway epithelial cells synthesize a leukocyte-adhesive hyaluronan matrix in response to endoplasmic reticulum stress. J Biol Chem. 2008; 283(38):26283–26296. [PubMed: 18644783]
36. Lauer ME, Fulop C, Mukhopadhyay D, Comhair S, Erzurum SC, Hascall VC. Airway smooth muscle cells synthesize hyaluronan cable structures independent of inter-alpha-inhibitor heavy chain attachment. J Biol Chem. 2009; 284(8):5313–5323. [PubMed: 19075022]
37. Kovacs EJ, Van Stedum S, Neuman JE. Selective induction of PDGF gene expression in peritoneal macrophages by interleukin-2. Immunobiology. 1994; 190(3):263–274. [PubMed: 8088855]
38. Morisaki N, Koyama N, Kawano M, et al. Human macrophages modulate the phenotype of cultured rabbit aortic smooth muscle cells through secretion of platelet-derived growth factor. Eur J Clin Invest. 1992; 22(7):461–468. [PubMed: 1516593]
39. Lindroos PM, Coin PG, Badgett A, Morgan DL, Bonner JC. Alveolar macrophages stimulated with titanium dioxide, chrysotile asbestos, and residual oil fly ash upregulate the PDGF receptor-alpha on lung fibroblasts through an IL-1beta-dependent mechanism. Am J Respir Cell Mol Biol. 1997; 16(3):283–292. [PubMed: 9070613]
40. Aono Y, Nishioka Y, Inayama M, et al. Imatinib as a novel antifibrotic agent in bleomycin-induced pulmonary fibrosis in mice. Am J Respir Crit Care Med. 2005; 171(11):1279–1285. [PubMed: 15735062]
41. Daniels CE, Wilkes MC, Edens M, et al. Imatinib mesylate inhibits the profibrogenic activity of TGF-beta and prevents bleomycin-mediated lung fibrosis. J Clin Invest. 2004; 114(9):1308–1316. [PubMed: 15520863]
42. Levitzki A, Mishani E. Tyrphostins and other tyrosine kinase inhibitors. Annu Rev Biochem. 2006; 75:93–109. [PubMed: 16756486]
43. Richeldi L, Costabel U, Selman M, et al. Efficacy of a tyrosine kinase inhibitor in idiopathic pulmonary fibrosis. N Engl J Med. 2011; 365(12):1079–1087. [PubMed: 21992121]

Europe PMC Funders Author Manuscripts

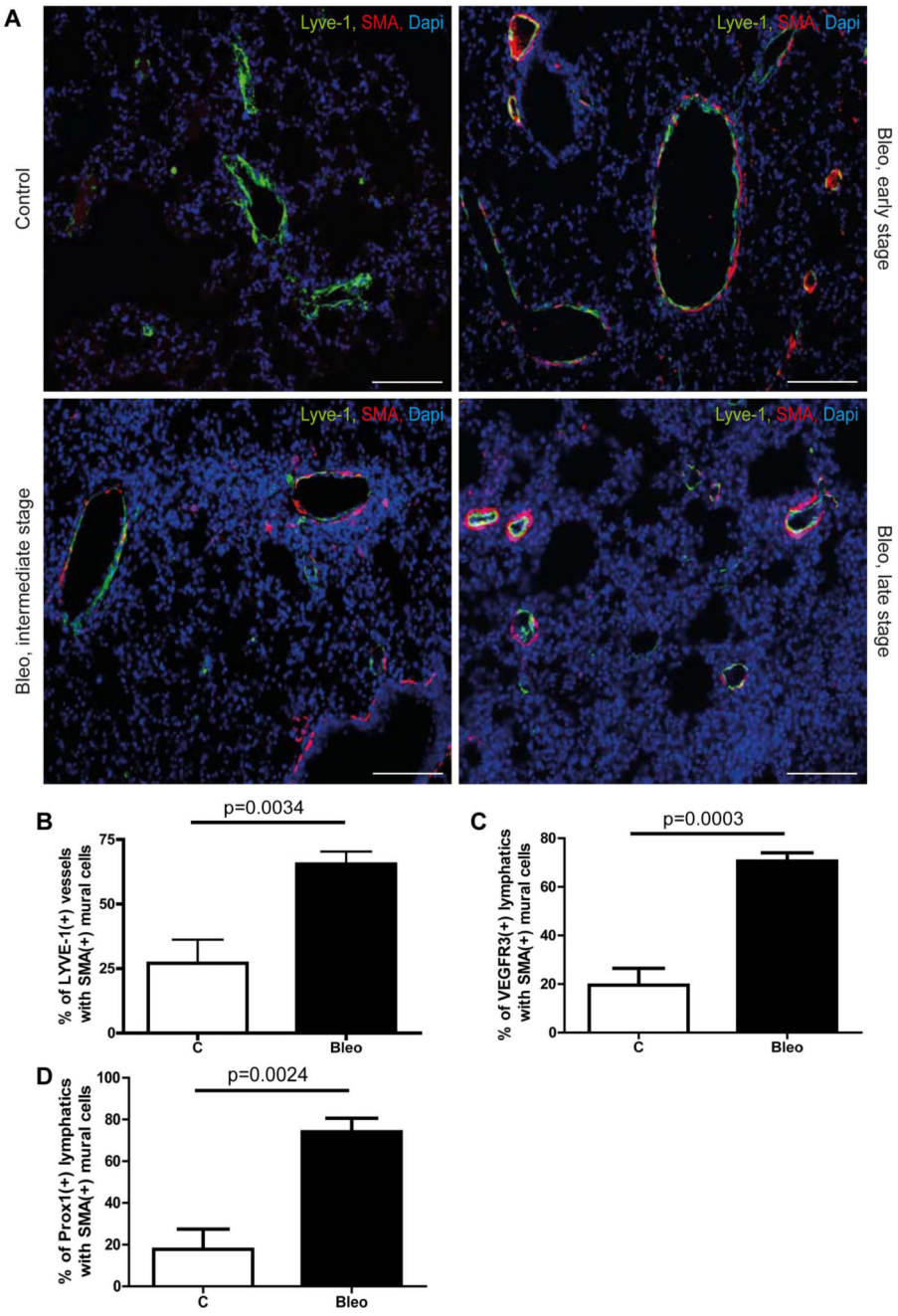

Figure 1. Aberrant recruitment of mural cells to lymphatic vessels during pulmonary fibrosis.

(A) Immunodetection of mural cells (SMA) and Lyve-1–positive vessels in fibrotic lungs of mice treated with bleomycin (Bleo; 10 mg/kg body weight twice a week intraperitoneally) and in healthy controls of mice treated with PBS (100 μL twice a week intraperitoneally) at day 28. Fibrosis is shown at early, intermediate, and late stage. Scale bars equal 100 μm. (B) Quantitative analysis of Lyve-1–positive vessels with SMA-positive mural cells in lung tissue of bleomycin-injected and healthy control mice at day 28 (controls n = 6; Bleo n = 8). (C) Quantitative analysis of VEGFR3-positive lymphatic vessels with SMA-positive mural

cells in lung tissue of bleomycin-injected and healthy control mice at day 28 (controls n = 5; Bleo n = 5). (D) Quantitative analysis of Prox1-positive lymphatic vessels with SMA-positive mural cells in lung tissue of bleomycin-injected and healthy control mice at day 28 (controls n = 5; Bleo n = 5). Error bars show SEM.

Europe PMC Funders Author Manuscripts

Europe PMC Funders Author Manuscripts

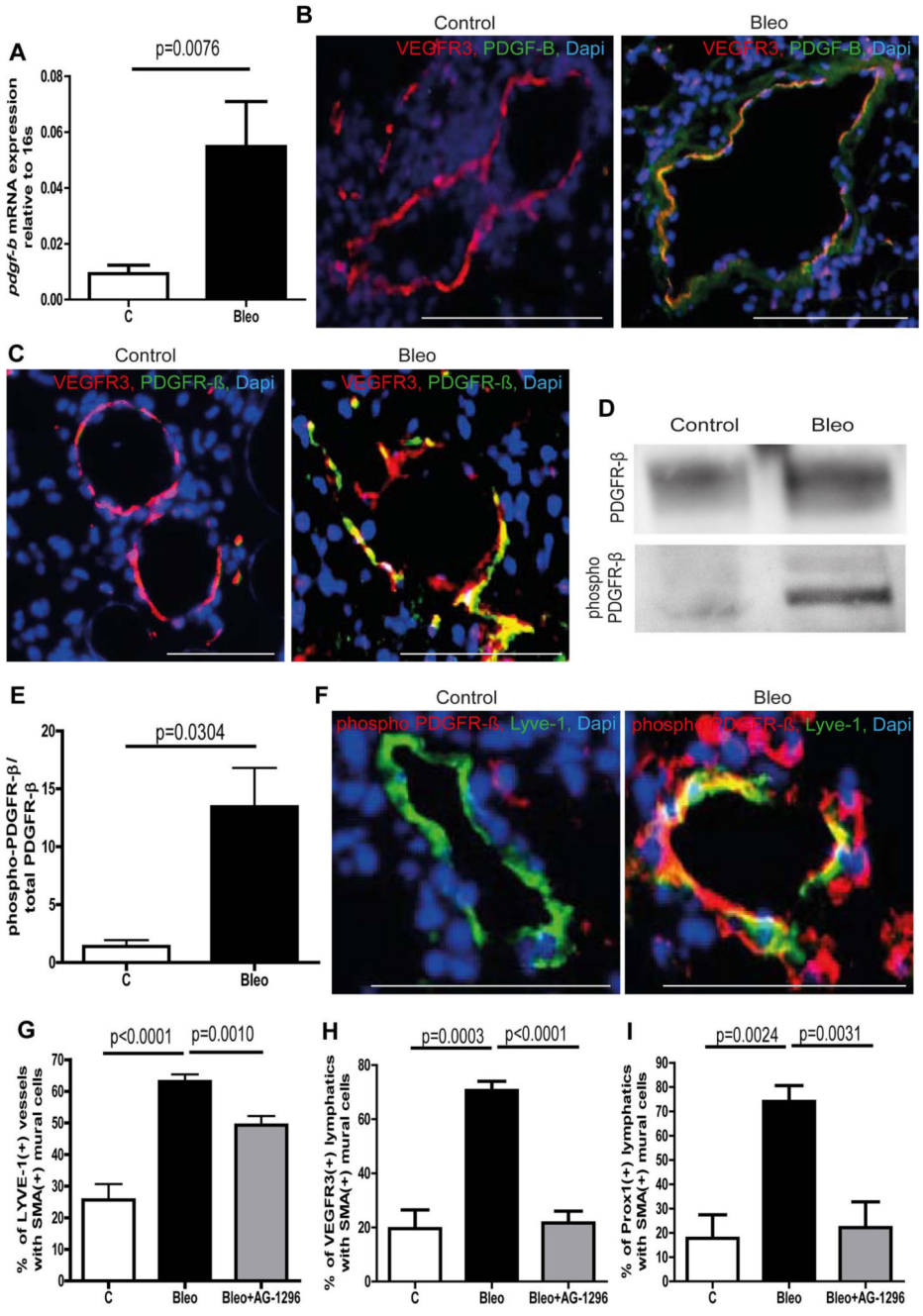

Figure 2. Ectopic expression of PDGF-B in lymphatic vessels and phosphorylation of PDGFR-β in mural cells leads to aberrant mural cell recruitment during pulmonary fibrosis.

(A) Quantitative analysis of the *PDGFR*-P expression in isolated lymphatic endothelial cells of bleomycin-treated (Bleo) and healthy control mice at day 28 (controls n = 15; Bleo n = 14). Immunostaining of PDGF-B (B) or PDGFR-β (C) and lymphatic vessels (VEGFR3) on lung tissue of fibrotic and control mice at day 28. Scale bars equal 100 μm. (D) Westernblot of phospho–PDGFR-β and total PDGFR-β of whole lung lysates at day 28 after treatment with bleomycin or PBS, respectively (controls n = 5; Bleo n = 13). (E) Quantitative analysis of the ratio of phospho–PDGFR-β to total PDGFR-β at day 28 after treatment with

bleomycin or PBS (controls n = 5, Bleo n = 13). (F) Double-immunodetection of phospho–PDGFR-β and lymphatic vessels (VEGFR3) on healthy and fibrotic murine lung tissue at day 28. Scale bars equal 100 μm. Quantitative analysis of Lyve-1–positive lymphatic vessels (G), VEGFR3-positive lymphatic vessels (H) or Prox1-positive lymphatic vessels (I) covered with SMA-positive mural cells at day 28 after treatment with bleomycin, bleomycin + AG-1296 (Bleo + AG-1296; 10 mg/kg body weight twice a week intraperitoneally; 0.5 ng, 5 times per week intraperitoneally, starting at day 14 after first bleomycin injection) or in healthy control lungs of PBS-treated mice (controls n = 15; Bleo n = 29, Bleo + AG-1296, n = 13). Error bars show SEM.

Europe PMC Funders Author Manuscripts

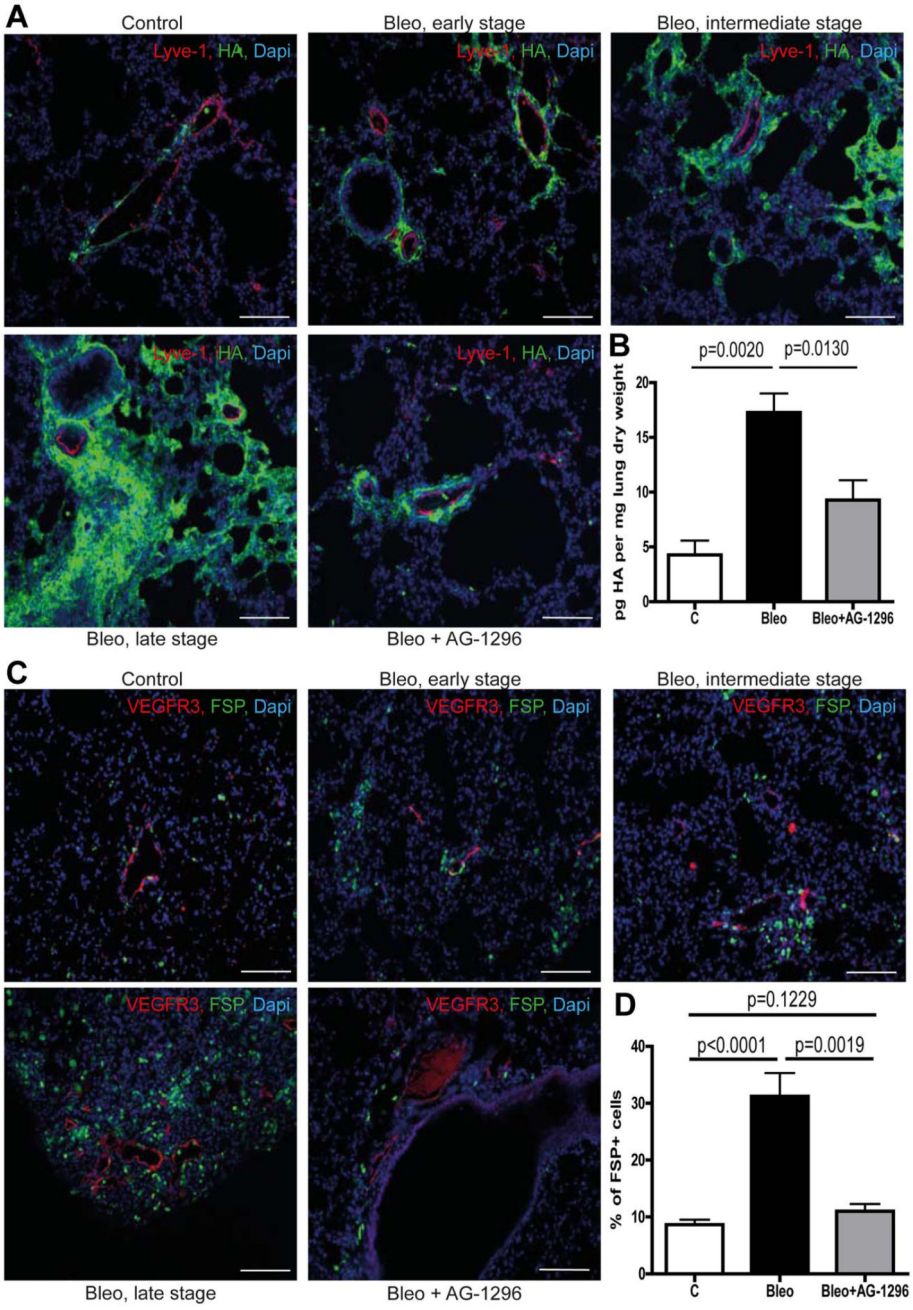

Figure 3. Aberrant mural cell recruitment results in perilymphatic accumulation of hyaluronan with subsequent formation of fibrotic lesions.

(A) Simultaneous immunodetection of HA and lymphatic vessels (Lyve-1) in fibrotic lungs of mice treated with bleomycin (Bleo), bleomycin + AG-1296 (Bleo + AG-1296) or in healthy control lungs of PBS-treated mice, respectively at day 28 on tissue of early, intermediate, and late stage fibrosis. Scale bars equal 100 μm. (B) Quantitative analysis of HA in lungs at day 28 after treatment with bleomycin, bleomycin + AG-1296 or PBS, respectively (controls n = 3, Bleo n = 6, Bleo + AG-1296 n = 6). (C) Immunodetection of fibroblasts (FSP) and lymphatic vessels (VEGFR3) in lungs of Bleo-, Bleo + AG-1296–, and

PBS-treated mice, respectively, on tissue showing early, intermediate and late stage fibrosis at day 28. Scale bars equal 100 μm. (D) Quantitative analysis of FSP-positive cells at day 28 in Bleo, Bleo + AG-1296, and PBS-treated mice, respectively (controls n = 15, Bleo n = 29, Bleo + AG-1296 n = 13). Error bars show SEM.

Europe PMC Funders Author Manuscripts

Europe PMC Funders Author Manuscripts

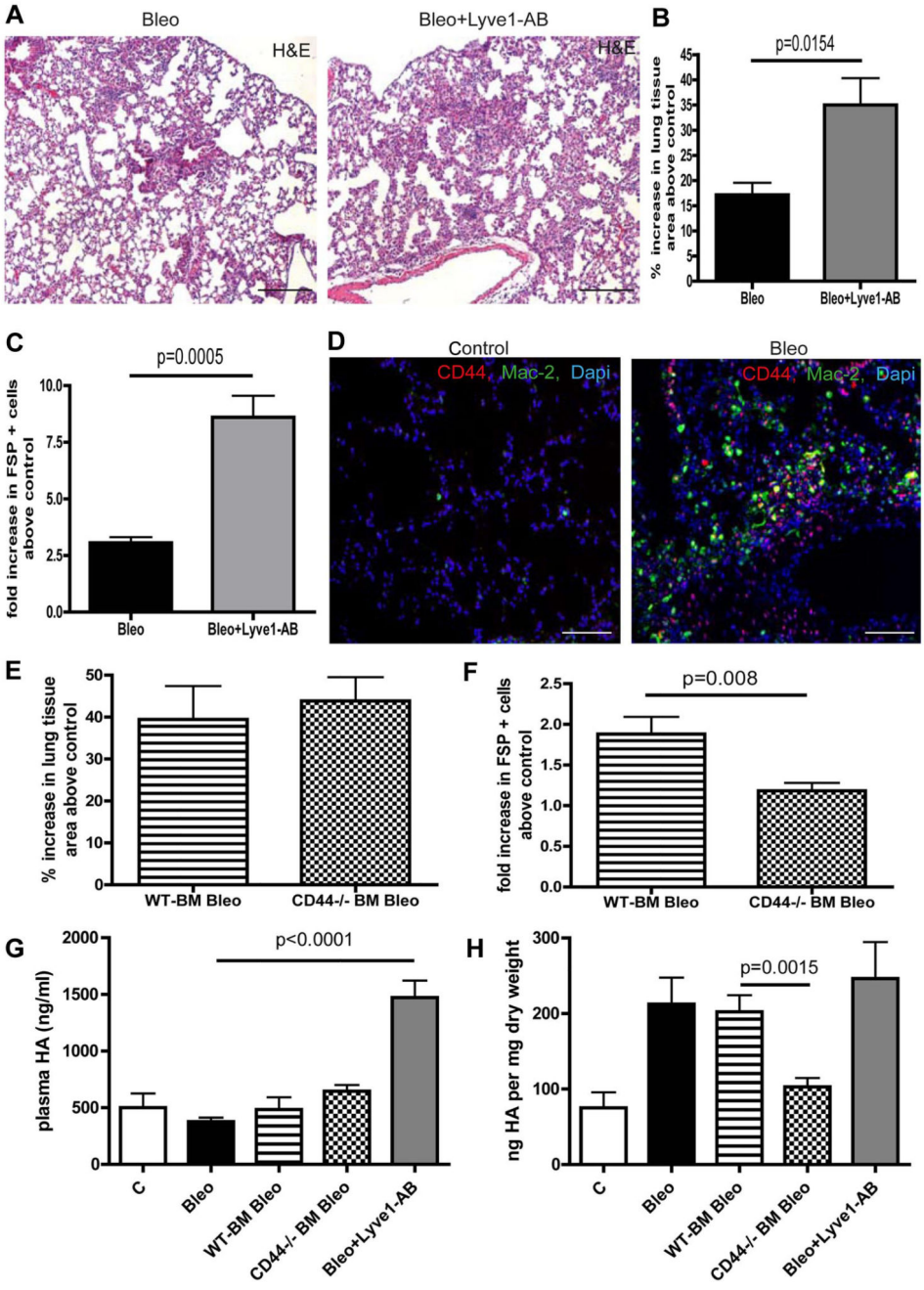

Figure 4. Various HA surface receptors contribute to HA clearance in the lung with different outcomes on pulmonary fibrosis.

(A) H&E histology on lung tissue of mice treated with bleomycin (Bleo; 10 mg/kg body weight twice a week intraperitoneally) or with bleomycin + Lyve1 antibody (Bleo + Lyve1-AB; (10 mg/kg body weight twice a week intraperitoneally; 100 μg Lyve1-AB 5 times every other day intraperitoneally, starting at day 15 after the first bleomycin injection) at day 28 (Bleo n = 5, Bleo + Lyve1-AB n = 5, control n = 2). Scale bars equal 200 μm. (B) Quantitative analysis of the percentage increase in the area of lung tissue of bleomycin and bleomycin + Lyve1 antibody-treated mice above PBS-treated control (100 μL twice a week

intraperitoneally) mice. (C) Quantitative analysis of FSP-positive cells on lung tissue Bleo and Bleo + Lyve1-AB–treated mice in comparison to control mice. (D) Immunodetection of CD44-positive cells (CD44) and Mac-2–positive macrophages (Mac-2) in lungs of PBS- (control) and bleomycin-treated (Bleo) mice at day 28. Scale bars equal 100 μm. (E) Quantitative analysis of the percentage increase in the area of lung tissue of mice that first received either wild-type (WT-BM Bleo) or CD44-deficient ($CD44^{-/-}$ BM Bleo) BM (recipients were irradiated with 10 gray, after 24 hours 5 X 10^6 BM cells of WT or CD44-deficient donor mice were injected intravenously into the tail vein) and were then treated with bleomycin (10 mg/kg body weight twice a week intraperitoneally, starting day 21 after transplantation) above PBS-treated control mice (control; recipients were irradiated with 10 gray, after 24 hours 5 × 10^6 BM cells of CD44-deficient donor mice were injected intravenously into the tail vein); 100 μL PBS twice a week intraperitoneally, starting day 21 after transplantation) mice (WT-BM Bleo n = 5, $CD44^{-/-}$ BM Bleo n = 7, $CD44^{-/-}$ BM PBS n = 4). (F) Quantitative analysis of FSP-positive cells on lung tissue of WT-BM Bleo and CD44-$^{-/-}$ BM Bleo mice in comparison with control mice. (G) Quantitative analysis of hyaluronan-levels (HA) in plasma at day 28 of PBS, Bleo, WT-BM Bleo, $CD44^{-/-}$ BM Bleo and Bleo + Lyve1-AB–treated mice. (H) Quantitative analysis of hyaluronan-levels (HA) in lungs at day 28 of PBS, Bleo, WT-BM Bleo, $CD44^{-/-}$ BM Bleo and Bleo + Lyve1-AB–treated mice. Error bars show SEM.

Europe PMC Funders Author Manuscripts

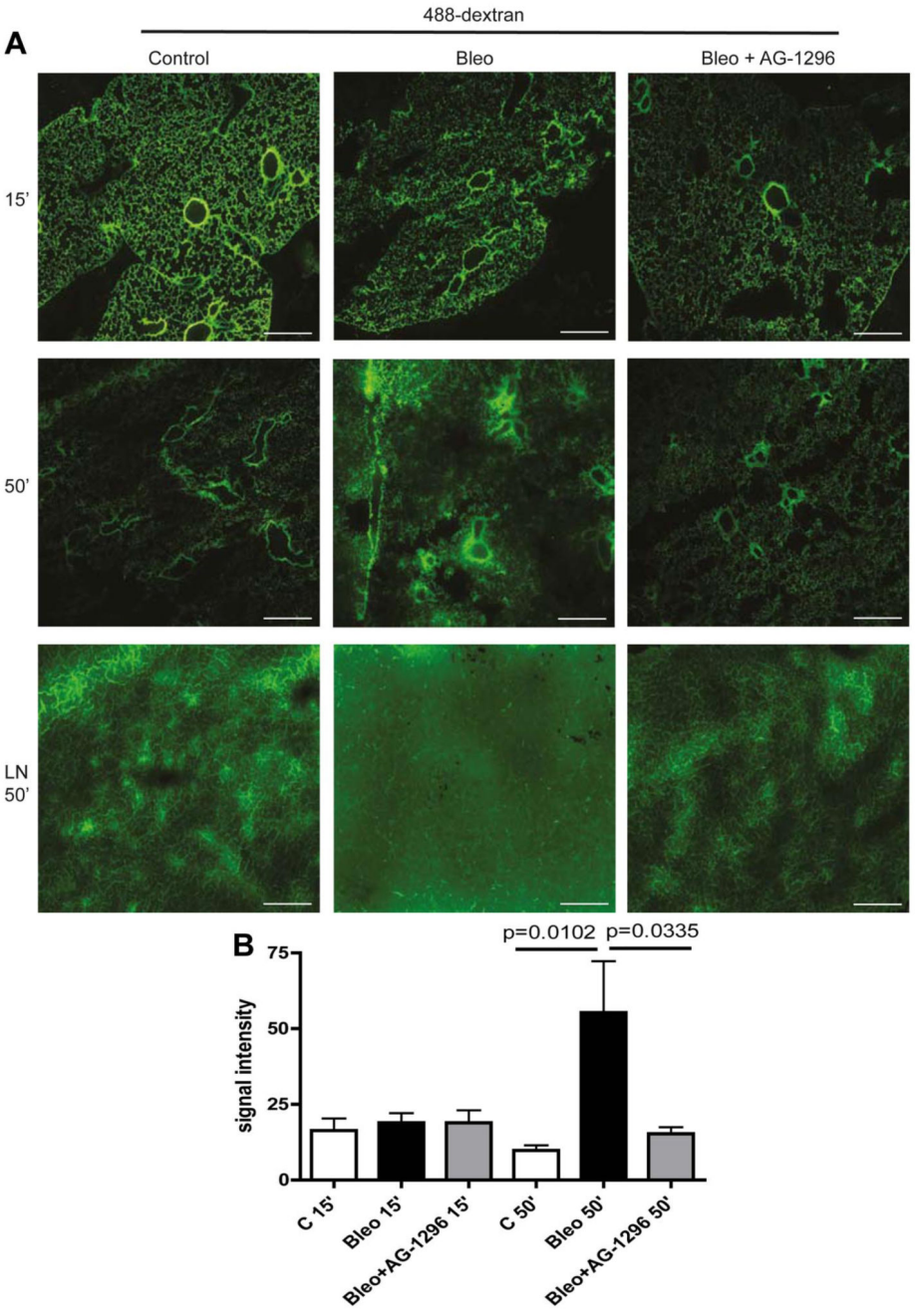

Figure 5. Aberrant mural cell recruitment to lymphatics leads to impaired lymphatic drainage of the lung and can be restored by inhibition of PDGFR-β–signaling.

(A) Fluorescence microscopy of 488-dextran (50 μL injected intratracheally at day 28) 15 and 50 minutes after injection in lung tissue of mice treated with bleomycin (Bleo), bleomycin+AG-1296 (Bleo + AG-1296) or in healthy control lungs of PBS-treated mice, respectively. Pretracheal lymph nodes (LN) were analyzed 50 minutes after 488-dextran injection. Scale bars equal 100 μm. (B) Quantitative analysis of the fluorescence signal intensity of 488-dextran measured with ImageJ in lung tissue of Bleo-, Bleo + AG-1296–, or

PBS-treated mice, 15 and 50 minutes after injection, respectively (n = 3 for each group). Error bars show SEM.

Europe PMC Funders Author Manuscripts

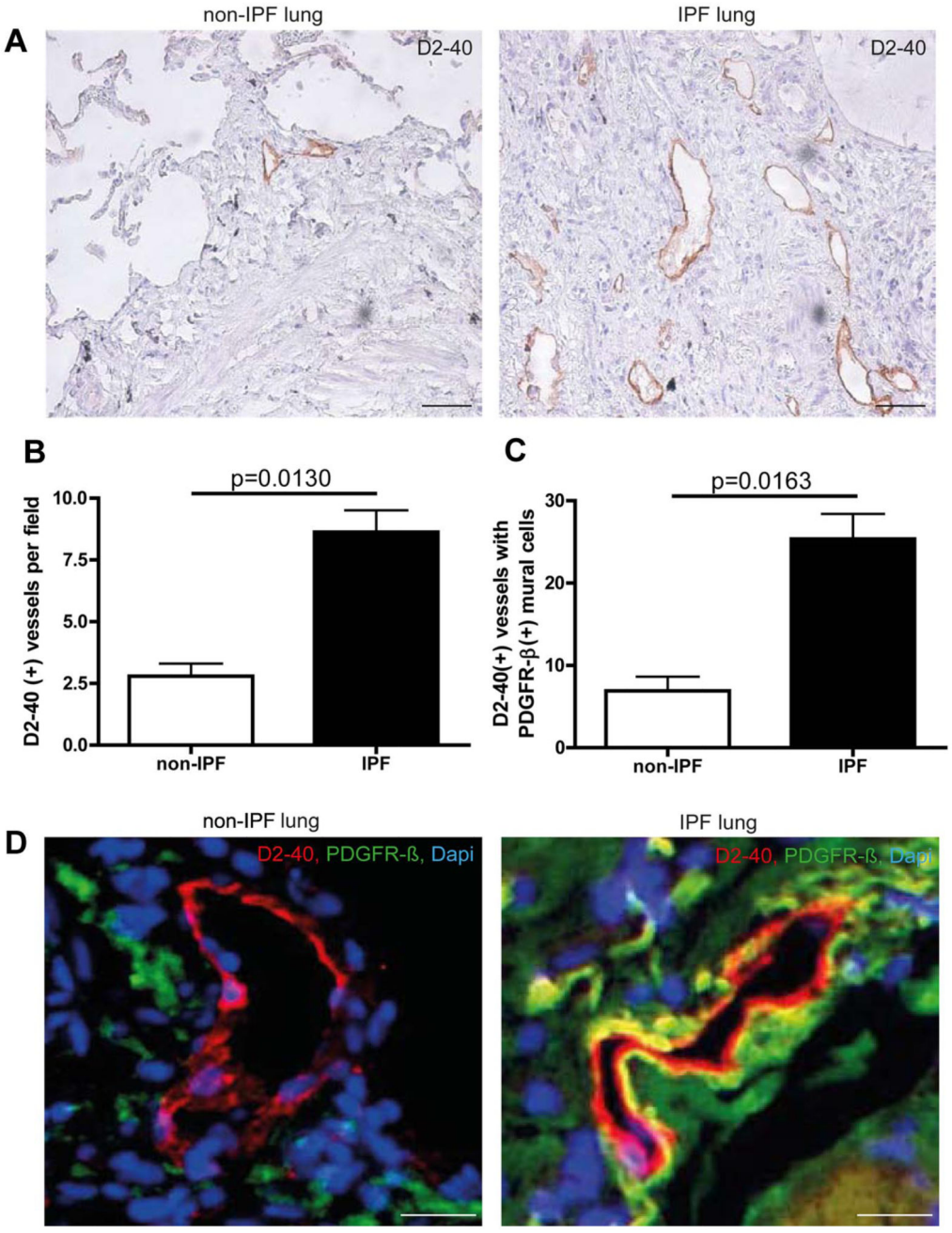

Figure 6. Aberrant mural cell recruitment in human IPF lungs.

(A) Immunohistochemistry of lymphatic vessels with the marker D2-40 on on-IPF lung tissue and IPF samples. Scale bars equal 200 μm. (B) Quantitative analysis of D2-40–positive vessels in lung tissue of IPF- and non-IPF patients (non-IPF n = 3, IPF n = 12). (C) Quantitative analysis of D2-40–positive lymphatic vessels associated with PDGFR-β–positive mural cells in lung tissue of IPF- and non-IPF–patients (non-IPF n = 3, IPF n = 12). (D) Simultaneous immunodetection of lymphatic vessels and pericytes, with the markers

Europe PMC Funders Author Manuscripts

D2-40 and PDGFR-β, on non-IPF lung tissue and IPF samples. Scale bars equal 50 μm. Error bars show SEM.

Europe PMC Funders Author Manuscripts